LAWRENCE
LIVERMORE
NATIONAL
LABORATORY

UCRL-JRNL-209327

Flow Around a Complex Building: Experimental and Large-Eddy Simulation Comparisons

R. Calhoun, F. Gouveia, J. Shinn, S. Chan, D. Stevens, R. Lee, J. Leone

January 31, 2005

Journal of Applied Meteorology

Flow Around a Complex Building: Experimental and Large-eddy Simulation Comparisons

Ronald Calhoun, Frank Gouveia, Joseph Shinn, Stevens Chan, Dave Stevens, Robert Lee, John Leone

Lawrence Livermore National Laboratory, Livermore, California

Corresponding author address: Ronald J. Calhoun, Arizona State University, Mechanical and Aerospace Engineering, PO Box 876106, Tempe AZ 85287-6106. Fax: 480 965-1384, E-mail: Ron.Calhoun@asu.edu

Abstract. A field program to study atmospheric releases around a complex building was performed in the summers of 1999 and 2000. The focus of this paper is to compare field data with a Large-Eddy Simulation (LES) code to assess the ability of the LES approach to yield additional insight in atmospheric release scenarios. In particular, transient aspects of the velocity and concentration signals are studied. The simulation utilized the Finite Element Method (FEM) with a high fidelity representation of the complex building. Trees were represented with a canopy term in the momentum equation. Inflow and outflow conditions were used. The upwind velocity was constructed from a log law fitted to velocites obtained on two levels from a sonic anemometer (2D) equiped tower. A number of different types of comparisons of the transient velocity and concentrations signals are presented - direct signal versus time, spectral, Reynolds stresses, TKE signals, and autocorrelations. While it is concluded that the LES approach does provide additional insight, the authors argue that the proper use of LES should include considerations of cost and may require an increased connection to field sensors, i.e., higher resolution boundary and initial conditions need to be provided to realize the full potential of LES. Otherwise, one may be easily misled by realistic signals which the LES naturally produces without yielding real insight.

1. Introduction

Flow and dispersion around buildings is becoming an increasingly important problem in the atmospheric sciences. This is due in part to the rapid urbanization of our population, and the enhanced perception of threats and catastrophes which affect urban populations. There has been significant and steady effort to understand these problems better (see, for example: Brown *et al.* 2001, Murakami 1993, Ramsdell 1998). Similation methods have been developed and applied extensively to model problems which are meant to capture some of the effects present in larger-scale atmospheric problems (see Calhoun & Street 2001, Ding *et al.* 2003, for examples). These efforts to understand and simulate "model" atmospheric problems have been productive due to careful measurements which can be obtained for these domains (see, for example, Snyder 1994, and Lawson *et al* 2000). Both Reynolds Averaged Navier Stokes Solutions (RANS) and Large-Eddy Simulations (LES) have been applied to these problems. In the following, the authors consider LES solutions compared to measurements taken during a field experiment. For a critical review of LES in the atmospheric sciences, see Mason (1994).

In the summers of 1999 and 2000, an experimental program was performed of atmospheric releases using a tracer gas around a complex building.

Surface energy budget stations, sonic anemometers (2D), and tracer gas samplers were used in the study. The overall goal of the experimental program was to provide better data for the evaluation of current modeling approaches to the prediction and analysis of atmospheric release scenarios on the individual building scale. There were several stages of the experimental program: 1. characterization of the mean wind fields, 2. providing averaged concentration measurements, 3. providing high resolution, transient wind and concentration data, 4. providing indoor concentration measurements concurrent with high quality outdoor measurements on the individual building scale. A previous paper (Calhoun *et*

al. 2004) has described in more detail stages 1 and 2. This paper is concerned primarily with stage 3.

The rationale behind this paper is to begin to better assess the contribution that the LES approach actually makes to modeling atmospheric releases. The experience of the authors has been that there are a number of particular challenges to effectively performing an LES approach. The first challenge is related to one of the strengths of LES - that transient signals can be easily and naturally produced. Therefore, most LES models will produce realistic looking transient signals. Because of the relative lack of high resolution transient data for flows over individual buildings, one is tempted to believe that the individual vortices and fluid mechanical details seen in the LES fields are close to real, that is, that they are approximately accurate in time and space.

Secondly, the LES approach degrades (apparently) gracefully as the resolution of the grids decrease. Even though typical formulations of LES expect that the subgrid-scale should begin in the inertial subrange of the turbulent cascade, realistic looking results (though perhaps different) may still be obtained with poor grid resolution. Therefore, it is possible to operate an LES model with the subgrid-scale model performing essentially as a Reynolds-averaged Navier Stokes (RANS) turbulence model, i.e., the effects of most of the energy containing eddies are not resolved, rather they are parameterized with the subgrid-scale model. To further complicate the issue, even an attempt to honestly resolve energy containing eddies in the main flow field will usually break down near the walls, since the energy containing eddies decrease in size as the wall is approached. Fortunately, there are currently attempts to clarify the proper roles of RANS and LES near walls and to create a hybrid approach; see literature on Detached-Eddy Simulation (DES), e.g., Travin *et al.* (2000), or Squires *et al.* (2001).

These challenges make the need for more detailed analysis of LES transient signals more pressing,

especially because of advances in computer power and modeling methods which will tend to make the LES approach more popular.

One might legitimately ask why, in addition to a statistical description, we explore the degree to which transient signals compare between the simulation and the measurements. While these flows are turbulent and hence display chaotic behavior in detail, the LES methodology might allow us to focus on the larger scales of motion and treat the smallest scales statistically through the use of the subfilter scale model. Hence, it is not inconceivable that the major portion of a signal describing a large vortex entering our flow domain might maintain some level of predictability across the domain. An increasing availability of real-time wind velocity information motivates our inquiry. For buildings important to a country's national security, arranging for real-time wind velocity information is relatively easy. The question becomes: Given real-time knowledge of wind direction shifts and variations in magnitude, can we improve modeling of flow and dispersion around buildings? Of course, in a mean sense, larger variations in wind direction can be related to larger horizontal eddy diffusivities. However, can, for example, an LES simulation capture a puff of airborne material that shifts to the other side of a building because of a ten second shift in wind direction from 180 to 210 degrees? Animations of LES fields would seem to indicate that this may be theoretically possible with this methodology. Many questions remain. For example, how much detail is required on the upwind flow boundary to allow an LES to capture some of these effects? Even if a real correlation between instantaneous velocities of the LES and measurements can not be demonstrated, can the approximate movement of larger puffs of gas be simulated with a useful degree of accuracy? We begin to explore these questions below.

2. Model setup and numerical methodology

2.1. Model setup

As described in Calhoun *et al.* 2004, an architecturally complex building was chosen as the site of the field experiment. In contrast, to results presented in Calhoun *et al.* 2004, however, this paper concerns only the final experimental day July 22, 2000. This was an intensive observation day with high speed wind stations, blue box samplers (SF_6 balloon sample boxes), and a Miran SF_6 real-time sampler.

Several important aspects of the simulation parameters are listed below (some of these are are similar to those in Calhoun et al. 2004, but others differ):

1) The flow was assumed neutral and no heat flux was imposed at the ground, representing cloudy, morning, or higher wind conditions. Consequently, only the experimental data which also represented neutral flow conditions was used in the following comparisons. The time of the year and conditions of the experiment were chosen so that neutral flow scenarios dominated for most of the duration of the experiment. Richardson number was used to determine if the flow was neutral based on an upwind sonic and energy budget station. Typically, this became a criterial requiring strong enough winds which did exist on July 22, 2000 at the experimental site.

2) Canopy effects (trees) were modeled with the addition of a drag term in the momentum equations. Both ornamental trees and a large row of Eucalyptus trees are modeled (see Figure **??**). We follow, for example, Yamada (1982) and add the following term to the mean momentum equations:

$$canopy\_drag = \eta C_d a(z) U|U|, \tag{1}$$

where η is the fraction covered by the canopy, C_d is the drag coefficient for the trees, $a(z)$ is the plant

area density, and U is the x component of mean wind speed. An analogous term is used in the y direction. Due to the desire to keep the subfilter-scale turbulence model simple, no enhancement of the subfilter turbulence due to the trees was implemented. Larger-scale enhancements to turbulence which could be resolved are naturally captured in the LES methodology. A standard value for the drag coeficient was taken from the literature (see Yamada 1982).

3) Wind directions were generally from the southwest of the building. Precise wind directions upstream of the building were acquired with a high-speed, sonic anemometer station. These speeds and wind directions were used to create an inflow profile (fitted to a log law) which was then used as input into the LES model. Incoming wind directions and speeds were updated every second from the sonic anemometer data.

4) Approximately 2.85 million grid points were utilized for the LES study. A fitted grid conforms precisely to the building shape. Marking some elements as belonging to a solid and others as in the fluid [easily done in FEM] prevented undue deformation in the grid. Stretching allowed the finest grid resolutions near the building to be approximately 40 cm. The computational domain spans 600 x 500 x 80 meters, where the smaller dimension is in the vertical direction. (Building height is about 10 meters on average, but about five different vertical levels exist.)

5) A Smagorinsky subgrid-scale turbulence closure was used. The Smagorinsky coefficient was set to 0.2 and the length scale was set to the cube root of the volume of the computational cells. The authors have experience utilizing the dynamic eddy viscosity model based on the Germano identity (see Calhoun & Street 2001), but it was decided to utilize the simplest LES turbulence model for the simulations presented here. However, it would be interesting to consider carefully the role of the subgrid-scale model in building-type atmospheric flows (see Tong *et al* 1999).

6) Approximately, ten minutes of the study was simulated. The first two minutes of the model run simulated the two minutes before the release at 6:30 p.m., and the final eight minutes simulated the first eight minutes of the release. Assuming an approximate speed of 5 m/s across a domain 500 m across, the approximate number of flow-through times (the time for a fluid parcel to travel from inflow to outflow) simulated was 6. Based on the authors experience with channel flows, this might be expected to yield converged values for low order statistics. A longer simulation time would naturally be preferable but cost was a consideration in these numerically intensive calculations.

7) The boundary conditions for the simulation were as follows. An inflow boundary was used upstream of the building and was formed by taking two levels of the velocity as measured by the sonic tower and fitting a log profile. An outflow boundary condition imposing zero gradient on the flow variables was used downstream. Outflow boundary conditions can have an effect upon the upstream flow near the outflow boundary (see, for example, Sani and Gresho 1994). To properly quantify this effect a series of simulations could be performed in which the outflow boundary is gradually moved downstream. Since these were expensive calculations, we used just two grids, one with a 400m x 400m x 80m domain, and a larger grid with a more distant downstream boundary (600m x 500m x 80m). Moving the outflow boundary condition downstream avoided difficulties associated with large eddies forming near the edge of the trees which occasionally caused backflow conditions near the boundary. The upper boundary condition was free slip. The lower boundary and on the building the LES used a wall-layer model dependent on distance to the wall. The roughness of the building surface was assumed to similar to that of concrete.

2.2. Summary of numerical methodology

The finite element method (FEM) used to solve the fluid dynamics and was described briefly in Calhoun *et al.* (2004), and with detail in Chan (1994) & Gresho and Chan (1998). The code used was developed at LLNL and is a modern CFD code for solving the time-dependent Navier-Stokes equations via the finite element method and a second-order projection method. The Poisson equation is solved via the multi-grid method using software available through LLNL's Center for Applied Scientific Computing (CASC). Time stepping uses a semi-implicit projection method which is second order accurate. An advantage of the FEM approach is its inherent capability, via the isoparametric element methodology, of performing simulations with complex geometry. For example, complex buildings can be naturally represented with the FEM approach.

The code was adapted for use on massively parallel computer platforms (Stevens et al., 2000) via MPI (Message Passing Inteface). The modeling framework is an object-oriented approach. It was originally developed for applications using the adaptive mesh refinement technique. It was modified to perform well on distributed memory computers while allowing the use of multiple dynamics drivers to customize the model to the problem of interest.

The simulations performed here used 256 processors of the ASCI White computer at LLNL. The computational domain spans 600 x 500 x 80 meters - a larger domain in the x and y direction (extensions to the east and north on the aerial photo) than that of the RANS simulations of Calhoun *et al.* (2004). Large eddies advecting down-stream made the outflow boundary condition unstable at shorter domain lengths.

3. Tracer Experiment

The mean wind fields around the building and an evaluation of a RANS computer model to simulate these fields were conducted in the summer of 1999 and presented in Calhoun *et al.* (2004). In the summer of 2000, a set of releases of an inert and almost neutrally buoyant gas (SF_6) was conducted around the building. Large-eddy Simulations were performed for the release experiment and are presented below. Figures 1 to 2 show photos of the experiment. In photo 2, the sonic anemometers can be seen mounted on tripods in the background. Notice the ornamental trees which complicate the flow scenario and the complex fascade of the building seen in photo 1. A smoke generator was used to gain visual insight into the dispersal patterns around the building (see photo 2).

Two types of samplers worked well in these experiments, a fast-response SF_6 sampler (Miran infrared spectrophotometer), and bag samplers (Blue Boxes) which collected air into mylar bags at preprogrammed intervals. Bag samples were processed by mass spectrometry after the experiment. The Miran instrument provides real-time, fast response SF_6 measurements. Data was sampled at one-second intervals, and databases are available for running 5-second averages for most of the experiments. However, for the July 22 experiment 1-second data resolution is retained in the database. After appropriate averaging, the two types of SF_6 measurements have been shown to compare quite well in a subsequent experiment in Salt City, October 2000 (Gouveia & Shinn, 2002).

Releases were conducted in the following manner. The smoke generator and data from the sonics were used to help find a good location for the source. Then SF_6 gas was released at some recorded and fixed rate (in the range of 2 to 18 grams/s) over the durations given in Table 2. A blower was used to mix the gas locally with a small volume of air as it was released. A summary of the experiments is provided in Table 1. As can be seen from Figure 4, July 22 was an intensive measurement day utilizing

both the Miran sampler and nine box samplers - each with 7 bags. The filling of the bags was controlled by synchronized on-box microprocessors and proceeded according to the schedule in Table 1.

Several comments may be of use to the reader who wishes to extend or corroborate the work presented here. First, because of the way that the sample boxes operate, i.e., with 30 seconds of purging before filling the balloons, the actual start time of the balloon sample is 30 seconds after the times listed above. The balloons were filled in 10 seconds and then closed. Secondly, although the data is not presented in this paper, bag samples were also collected inside the building to better understand how gases may penetrate the building shell and ventilation systems. For the inside sample boxes, the 6th and 7th bags were filled at later times - in anticipation that the building would "store" SF_6 even after outside levels were quite low. Interested readers should contact the authors to access the data. Data from the energy budget station showed that for our conditions, the wind speed was strong enough for shear forces to dominate buoyancy forces. Therefore the flow is treated a neutrally buoyant in the simulation.

Figure 3 is a summary map of all the release points, SF_6 sampling locations, and sonic anemometer stations. Figure 4 shows experimental setups for July 22, 2000. On July 8 and 9, 2000, the source was located off the southern and western corner of the building and the sampler was on the south side of the building. From Table 2, one can see that on July 9, there were a series of 3 minute continuous point releases. The sampler seen in the map should be assumed to be the Miran sampler unless specified as a blue box sampler (bag sampler) on July 22.

4. Experiment and data collection

Figure 4 (repeated from Calhoun *et al.* 2004 for convenience) shows the experimental setup on July 22, 2000. Each of the stations labeled HS are a sonic anemometer mounted on a tripod with a high speed data acquisition system which recorded velocity data every second. No onbox averaging was used at this time. Note that the HS tower upstream of the building contained two sonic anemometers at 4.4 and 8.8 meters above the ground. The site marked "EB Station" refers to the Energy Budget station which was used to gather data on atmospheric stability. The Miran sampler also recorded data at the frequency of once per second. The blue box samplers filled each of their seven mylar balloons 30 seconds after the time listed for the bag number in Table 1. The heights of the instrumentation for the July 22, 2000 experiment are show in Table 3.

5. Model - experimental comparisons

Figure 5 illustrates several characteristics of the LES solution. An isosurface of concentration is shown, colored by wind speed. First, note the highly varying and transient solution. Animations of this and other views have been made by the authors. Secondly, notice how there are higher wind speeds, as should expected, for the gap in the trees (higher speeds are represented by warmer colors, slow speeds are represented by colder colors). It also appears that this isosurface is pulled downwards after passing through the line of Eucalyptus trees.

Before looking at the high frequency data, it is useful to view the ten minute averaged data as presented in Figure 6. HS 1, 2, and 5 all have significantly lower wind speeds, which clearly is caused by the fact that they are placed in recirculation zones, partially sheltered from the wind by the building. Between 18:30 and 18:40, the strongest winds are for HS station 7 which is located on top of the

building. Wind directions, shown in Figure 7, show a dramatic shift in direction for HS station 5, while the other stations appear much more stable. HS 5 is in a location near the northwest corner of the building where gradients are strong and minor shifts in wind direction or position can mean the difference between being located in the recirculation behind the corner or in the free-stream.

Upstream wind speed and direction for both the 4.4 meter and the 8.8 meter height showed the expected increase in speed with height, and there did not appear to be systematic differences in wind direction between the two upstream heights - as one would expect in neutral conditions. The strongest winds during the experiment typicall came from approximately 245 degrees. Winds directly from the south are at 180 degrees, and winds from west are at 270 degrees. Therefore, the strongest winds are between these two, approximately out of the southwest, and, not coincidentally, aligned with the skewed direction of the north edge of the building. The building shields HS 5 from the front when winds come from a more southerly direction, and blocks the flow from the back when winds are more northerly, creating a stagnation area with slower wind speeds.

5.1. Comparisons of high frequency velocity signals

Comparisons between high frequency signals of the velocity do not in general correlate well. Visual inspection of simulated versus sonic data for high speed station 7 are shown in Figure 8. In the recirculation zones, individual turbulent events do not compare well between the experiment and the model. The signals compare better for HS 7. This may be because the original high correlation between the sonics and the inflow boundary condition has not traveled through any large wake or recirculations zones. These signals show, in general, a tendency of the model to have overly dramatic variances - an impression that is corroborated by statistical analysis in the next section. One might speculate that the

eddy viscosity of the subgrid-scale model could be too low. The means appear reasonable in most of the signals, except HS 6 where there is clearly both larger variances and too low an average magnitude for the u component of velocity. HS 6 is located in a very challenging region to model correctly, i.e., a high gradient region lies near the edge of a recirculation zone and outer, near ambient flow velocities. An error in location either of the numerical gridpoint or the sonic location will produce large errors in the signal.

5.2. Variances and covariances in the velocity signals

A statistical analysis presented in Table 4 corroborates most of the impressions from a visual inspection of the signals. The means compare reasonably for all except HS 6 as explained above. The variances are systematically high for the model. Though some are better or worse, most variances compare within a factor of 2 or 3. In addition, the linear correlation coeficient is quite low in the recirculation zones, indicating that the model can not be considered predictive on an individual eddy by eddy basis. The linear correlation coeficient is defined:

$$r_{LES-Sonic} = \frac{\overline{(LES)'(Sonic)'}}{\sqrt{\overline{(LES)'(LES)'}}\ \sqrt{\overline{(Sonic)'(Sonic)'}}}.$$

5.3. Spectral analysis

Figures 9 through 11 plot frequency versus discrete spectral energy. From the spectral perspective, the comparisons appear reasonable indicating that the model distributes energy among the various scales of eddy motions in a way that is roughly similar to that measured. In some cases, similar peaks in the spectrum appear when comparing model versus measured data. For example, HS 1 has peaks in both the sonic and LES data of magnitude approximately 0.17 between .02 and .03 Hertz. Though it

is important to keep in mind the the fundamental equivalency between signals in physical and spectral space, the spectral perspective would, nevertheless, seem to indicate that the approximate shape of the distributions can be reproduced by the model.

5.4. UV - event plots

UV-event plots, seen in Figures 12 through 17, also seem to indicate that some features of the turbulence resolved in the model have important similarities with measured data. As demonstrated through the roughly symmetrical cloud of points distributed around the axes for stations HS 1 and 2, both the model and the sonics indicate that the turbulence has a more isotropic character at these locations. The skewness of the distributions of HS 5,6, and 7 shows that the model is roughly capturing an aspect of the flow physics, i.e., the type of anisotropy. For example, even though in Figure 15, the uv-events are distributed not densely enough around the origin, the type of anisotropy is clearly reproduced.

5.5. Autocorrelations

Autocorrelations in time, $\overline{u(t)'u(t+\tau)'}/(\overline{u'u'})$, have been calculated and are displayed in Figures 18 through 21. The idea behind this calculation is to learn over what length of time a signal is correlated with itself. This provides a measure of the size (in terms of time) of the largest energy containing eddies. The model produces quite similar behavior compared to the measured signals. For example, in Figures 18 and 19, both model and experimental data show a drop of the correlation to zero at approximately 7 seconds. In general, the signals decorrelate, roughly, with 10 to 20 seconds time shifts. This is consistent with the spectral analysis which showed the most energy from 0 to .05 Hertz (.05 cycles per second equals 20 seconds per cycle).

5.6. TKE

The TKE (2d) plots shown in Figures 22 suffers from similar discrepancies as the variances above. Namely, the model overestimates the TKE and produces overly dramatic swings in the signal. Of course, it is to be expected that problems producing high quality variances would propagate to the TKE plots since TKE is a function of the variances. Note that, traditionally, TKE is defined as: $\frac{1}{2}(\overline{u'u'} + \overline{v'v'})$.

The spatial distribution of 2d TKE can be seen in Figure 23. [North is directly up in the graph. The vertical level of the graph is at 2.5 meters above the ground.] Regions of high TKE exist in and directly downstream of both gaps in the row of trees to the east of the building. This is expected since there are higher velocities through the gaps. Notice, as well, that two other regions of high TKE are located on the north side. One is on the north-west corner as the flow must turn around the building, and the other is north of the north-east corner. The drag effects of the ornamental trees north, south, and east of the building can be seen as slow/blue regions with a circular shape. The model predicts relatively high TKE on the northeast side of the inner courtyard and low TKE near the southeast corner.

5.7. Concentrations

Comparisons with the blue box sampler data are shown in Figures 24 through 29. Three items are plotted in these graphs: the LES concentration curve, circle symbols representing the blue box data, and boxes representing appropriate averaging of the LES concentration data for comparisons with blue box data. Notice that the concentrations comparisons are quite good. The model predicts near zero concentrations in the same places and times that the samplers found near zero concentrations.

In Figure 27, the averaged LES concentrations at about 320 seconds does measure more SF_6 present; however, the unaveraged LES concentration curve shows a very good match with the data. It is clear from the sharp spike in the LES concentration data, that averaging a slightly earlier section of the signal would produce the near zero level measured. Likewise, when the samplers measured more significant concentrations of SF_6, the model produces impressively similar levels. For example, in Figures 28 and 29, the model accurately produces both the magnitude and timing of the measured spike in SF_6 (see 320 seconds in both plots). Note that no significant levels of SF6 were measured by blue boxes 12,18, and 23. At these locations, the model also predicts no significant levels of SF6.

It is even more interesting to compare the SF_6 concentration measured by the Miran real-time sampler with the LES data (Figure 30). The initial onset, the magnitude, and the duration of the initial peak of tracer gas is accurately simulated. The second and third peaks of SF_6 are also approximately correct in both timing and magnitude. After this, there was an unfortunate gap in the Miran data due to instrument problems.

6. Conclusions

The purpose of this paper was to assess the ability of an LES model to usefully add insight for flow scenarios around single buildings. Detailed results have been presented comparing SF_6 sampler data, high speed sonic anemometer data, and simulated data. The simulation clearly captured some aspects of the turbulence produced in the experiment, i.e., type of anisotropy, spectral characteristics, and the length of time for signals to decorrelate. However, the model did not perform nearly as well in the calculation of variances. Often the mean values were acceptable, but the model produced exaggerated swings in the signal and has not shown high correlations between the measured and modeled wind

speed signals. This was particularly true for the recirculations zones, where all of the high speed sonic anemometer stations were placed, with the exception of HS 7 which was located on the roof. Consequentially, the TKE comparisons had similar discrepancies. Despite these limitations, however, simulated concentrations matched closely the measured concentrations. In particular, these results suggest that high-resolution computational fluid dynamics models hold promise for adding insight into the onset, strength, and duration of transient atmospheric releases for single or multiple building scenarios.

The following recommendations might be suggested. First, it is clear that LES is a numerically expensive and complex option and may be easily misused. Previously, it has been shown (Calhoun *et al.* 2004) that RANS and Gaussian approaches yield useful results, perhaps more than commensurate with their level of effort. Therefore, more complex models should perhaps be used in more specialized circumstances, where the luxury of additional time and effort can be afforded. Still, the complex model does appear to add valuable insight, and the difficulty in the calculation of variances might be addressed with a more accurate subgrid-scale model. Also, evidence from this study suggests that correctly capturing detailed eddy evolution is at the very least extremely challenging with the boundary condition used here. More information is likely required on the inflowing turbulence before LES can be expected to yield higher correlations between experiment and simulation on an eddy to eddy basis. As to be expected, statistical properties such as spectral energy density, spatial decorrelation lengths of eddies, and level of anisotropy are easier to capture than transient signals. Does it make sense to use a data stream from upstream sonics combined with LES-style modeling to better characterize transient aspects of flow and dispersion around buildings of high interest? Some evidence from the SF6 experiment-model comparison given here suggests that at least in the near field there is some possibility

of useful model results. Clearly, improved upstream information is a priority, as is reseach on how best to filter or extend upstream data to create an upstream boundary condition.

Second, field experiments would appear to be essential toward the goal of improving computational fluid dynamics approaches. As faster computers increasingly allow more complex modeling methods, it will become more important to accurately understand boundary and initial conditions. In the above study, for example, the varying, inflow boundary, created from real sonic anemometer data, gave the LES a higher degree of realism. However, better boundary conditions should be explored, preferably incorporating data streams rich in spatial as well as temporal information.

Third, real-time tracer samplers vastly improve the ability to evaluate complex models. The Miran sampler performed well in the experiment, and one might imagine a future test with multiple real-time samplers deployed not only in the front of the building but also in the recirculations zones.

Acknowledgments. Special thanks are due to the outstanding computer consultants at LLNL, Mark Seager, and LLNL's Frost Science Runs Program. This work was performed under the auspices of the U.S. Department of Energy by the University of California, Lawrence Livermore National Laboratory.

This work was performed under the auspices of the U.S. Department of Energy by University of California, Lawrence Livermore National Laboratory under contract W-7405-Eng-48.

References

Brown, M., M. Leach, R. Calhoun, S. Smith, D. Stevens, J. Reisner, R. Lee, S. Chin, and D. DeCroix, 2001, Multiscale modeling of air flow in Salt Lake City and the surrounding region, ASCE Structures Congress, Washington, DC.

Calhoun, R., and R. Street, 2001, Turbulent flow over a wavy surface. Part 1: Neutral case, Journal of Geophysical Research, 106, C5, 9277-9293.

Calhoun, R., S. Chan, R. Lee, J. Leone, J. Shinn, and D. Stevens, 2004, Flow around a complex building: Comparisons between experiments and a Reynolds-averaged Navier-Stokes approach, Journal of Applied Meteorology, 43, 696-710.

Calhoun, R., R. Cederwall, D. Stevens, and R. Street, 2000, Highly resolved LES of the stable boundary layer over terrain, 14th AMS Symp. Bound. Layers & Turb., Boulder, CO.

Chan, S., 1994, An improved three-dimensional heavy-gas dispersion model: User's Manual, UCRL-MA-116567 Rev. 1, Lawrence Livermore National Laboratory.

Ding, L., R. Calhoun, and R. Street, 2003, Numerical simulation of strongly stratified flow over a three-dimensional hill, Boundary-Layer Meteorology, 107, 81-114.

Gouveia, F. and J. Shinn, 2002, Dense network of near-field observations of building-canopy winds and tracer concentrations during the Urban 2000 Experiment, 4th Symposium on the Urban Environment, Norfolk, VA, 180-181.

Gresho, P., and S. Chan, 1998: Projection 2 goes turbulent - and fully implicit, *J. Comp. Fluid Dyn*, 9, 249-272.

Lawson, R., S. Perry, and R. Thompson, 2000, Measurement of velocity and concentration fields in arrays of 2-dimentional and 3-dimensional buildings in a simulated neutrally-buoyant atmospheric boundary layer, USEPA FMF data report.

Mason, P., 1994, Large-eddy simulation: A critical review of the technique, Q. J. R. Meteorol. Soc., 120, 1-26.

Murakami, S., 1993, Comparison of various turbulence models applied to a bluff body. Journal of Wind Eng.

Ind. Aerodyn., 46&47, 21-36.

Ramsdell, J., and C. Fosmire, 1998, Estimating concentrations in plumes released in the vicinity of buildings: model development, Atmospheric Environment, 32, 10, 1663-1677.

Squires, K., J. Forsythe, and P. Spalart, 2001: Detached-Eddy Simulation of the separated flow around a forebody cross-section, *Direct and Large-Eddy Simulation IV, ERCOFTAC Series*, Volume 8, B.J. Geurts, R. Friedrich and O. Metais, editors, Kluwer Academic Press, 481-500.

Sani, R., and P. Gresho, 1994, Resume and remarks on the open boundary condition minisymposium, International Journal for Numerical Methods in Fluids, 18, 983-1008

Snyder, W., 1994, Some observations of the influence of stratification on diffusion in building wakes, Stably Stratified Flows: Flow and Dispersion over Topography, I.P. Castro and N.J. Rockliff (Eds.), 325-358.

Stevens, D., A. Almgren, J. Bell, V. Beckner, and C. Rendleman, 2000, Small scale processes and entrainment in a stratocumulus marine boundary layer, Journal of the Atmospheric Sciences, 57, 4, 567-81.

Tong, C., J. Wyngaard, and J. Brasseur, 1999, Experimental study of the subgrid-scale stresses in the atmospheric surface layer, Journal of the Atmospheric Sciences, 56, 2277-2292.

Travin, A., M. Shur, M. Strelets, and P. Spalart, 2000: Detached-eddy simulations past a circular cylinder, *Flow,-Turbulence-and-Combustion*, 63, 1-4, 293-313.

Yamada, T., 1982, A numerical model study of turbulent airflow in and above a forest canopy, Journal of the Meteorological Society of Japan, 60, 1, 439-454.

Received _____

Submitted to the *Journal of Applied Meteorology*, 2003.

List of Captions

Figure 1. North side of the building.

Figure 2. Side view of fogger release in front of the building.

Figure 3. Summary map for locations of releases, samplers, and anemometers.

Figure 4. Instrument deployment map for July 22.

Figure 5. Simulated SF6 Release. Isosurface of concentration colored by windspeed.

Figure 6. Ten minute averages of wind speed for all HS stations July 22, 2000.

Figure 7. Ten minute averages of wind direction for all HS stations July 22, 2000.

Figure 8. Simulated vs measured u component of velocity - high speed station 7.

Figure 9. Spectra intensity v: simulated vs measured - high speed station 1.

Figure 10. Spectra intensity u: simulated vs measured - high speed station 2.

Figure 11. Spectra intensity u: simulated vs measured - high speed station 7.

Figure 12. uv events: simulated - high speed station 1.

Figure 13. uv events: measured - high speed station 1.

Figure 14. uv events: simulated - high speed station 5.

Figure 15. uv events: measured - high speed station 5.

Figure 16. uv events: simulated - high speed station 7.

Figure 17. uv events: measured - high speed station 7.

Figure 18. Autocorrelations of u in time: simulated - high speed station 1.

Figure 19. Autocorrelations of u in time: measured - high speed station 1.

Figure 20. Autocorrelations of u in time: simulated - high speed station 2.

Figure 21. Autocorrelations of u in time: measured - high speed station 2.

Figure 22. $\frac{1}{2}(\overline{u'u'} + \overline{v'v'})$: simulated vs measured - high speed station 5.

Figure 23. $\frac{1}{2}(\overline{u'u'} + \overline{v'v'})$: simulated. The vertical level of the norizontal plane depicted is 2.5 meters above the

ground.

Figure 24. Concentrations of SF6 (ppb): simulated vs measured - BlueBox station 1.

Figure 25. Concentrations of SF6 (ppb): simulated vs measured - BlueBox station 4.

Figure 26. Concentrations of SF6 (ppb): simulated vs measured - BlueBox station 17.

Figure 27. Concentrations of SF6 (ppb): simulated vs measured - BlueBox station 24.

Figure 28. Concentrations of SF6 (ppb): simulated vs measured - BlueBox station 39.

Figure 29. Concentrations of SF6 (ppb): simulated vs measured - BlueBox station 45.

Figure 30. Real-time SF6 sampler vs LES - concentrations of SF6 (ppb). (Time range where both sets of data are available is shown.)

Figure 1. North side of the building.

Figure 2. Side view of fogger release in front of the building.

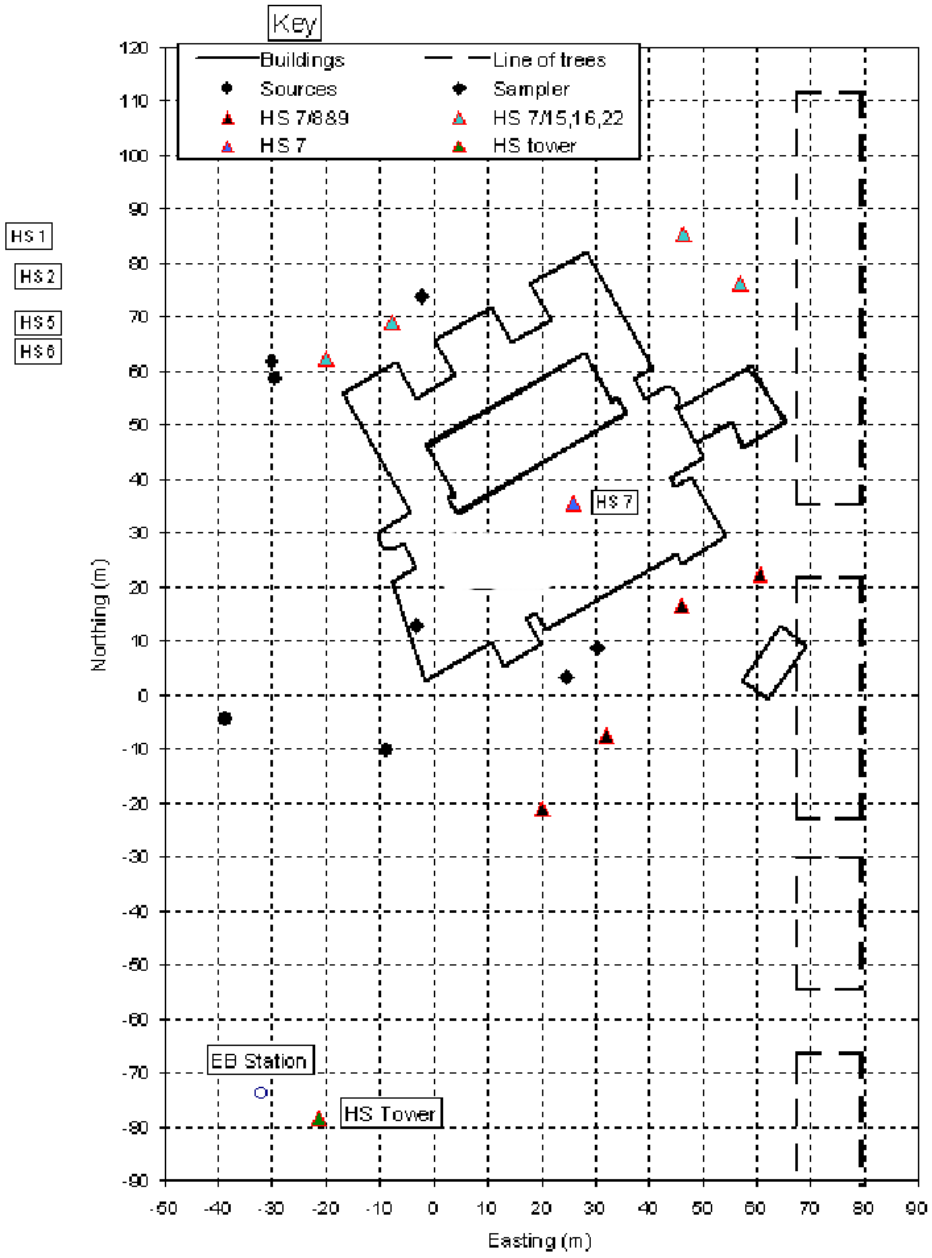

Figure 3. Summary map for locations of releases, samplers, and anemometers.

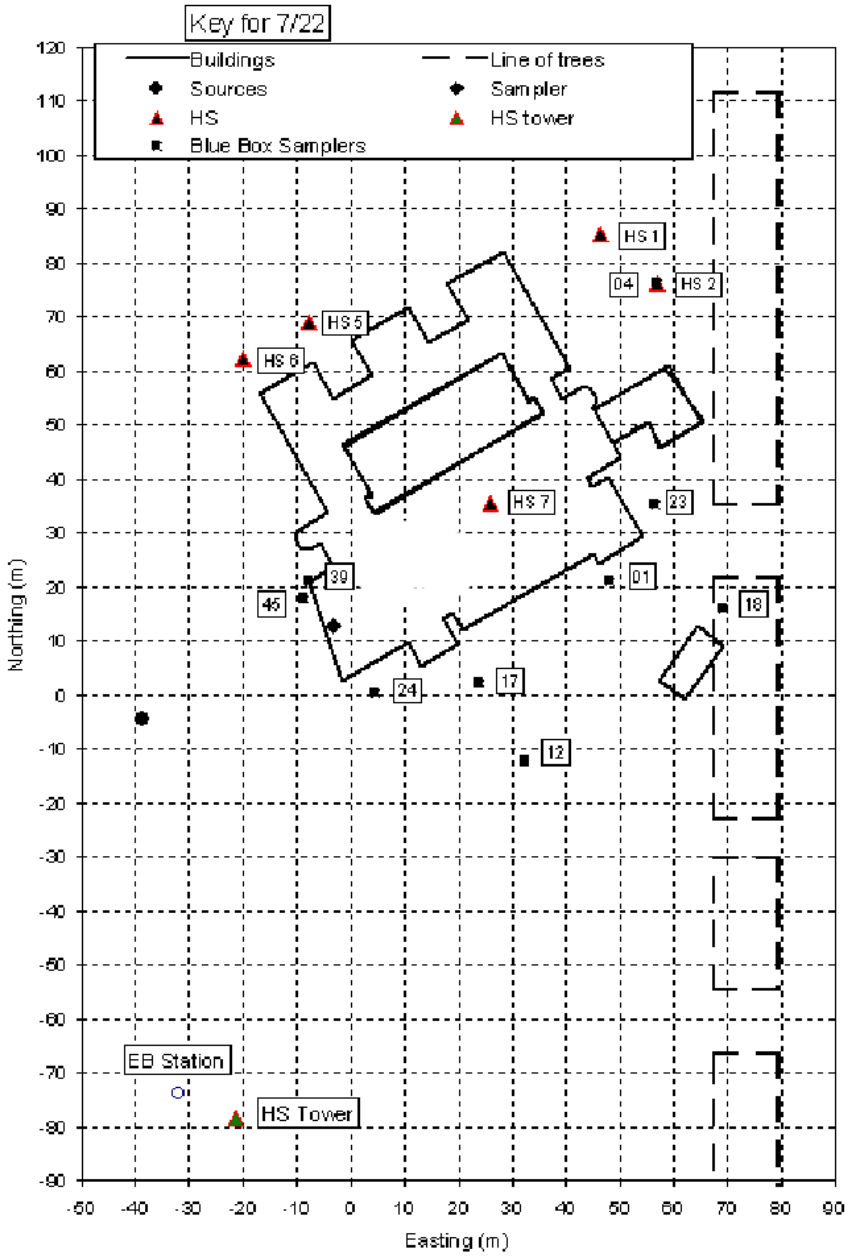

Figure 4. Instrument deployment map for July 22. EB represents the energy-budget station, and HS refers to locations of high-speed sonics. The fast response SF6 (Miran) sampler is located at the southwest corner of the building as designated by the diamond.

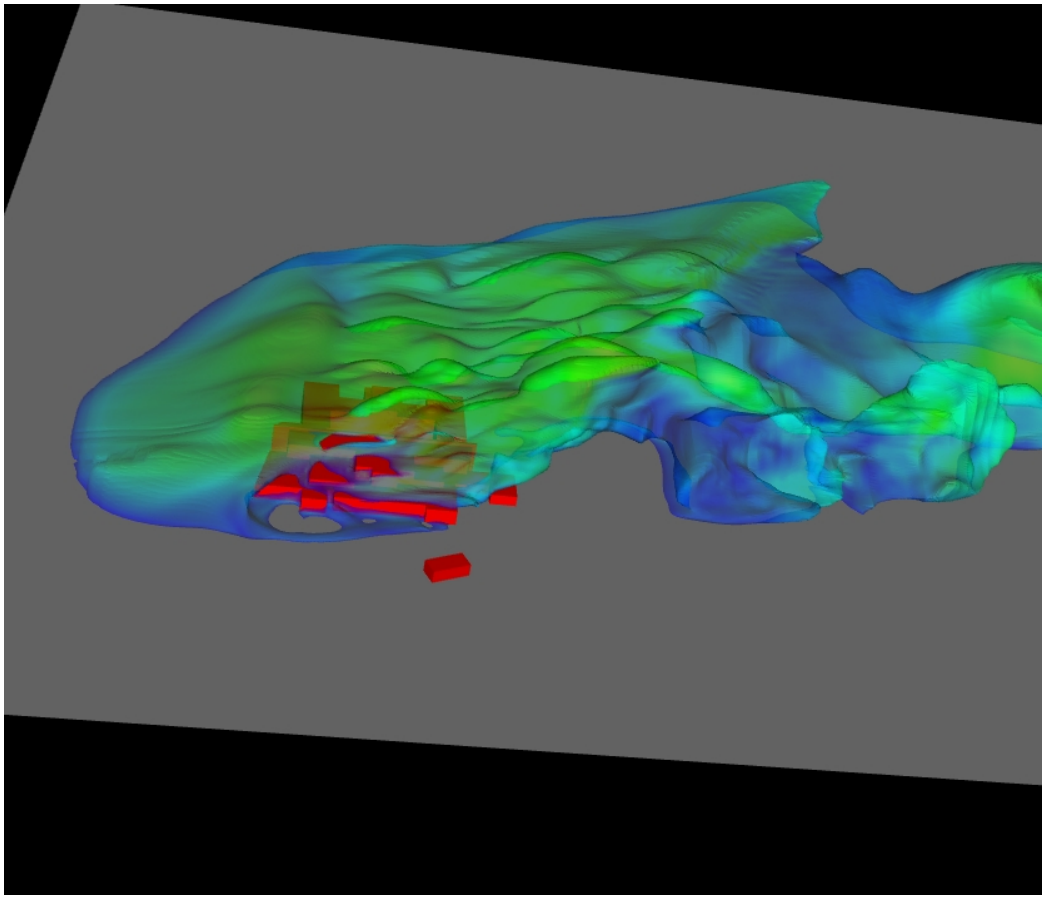

Figure 5. Simulated SF6 Release. Isosurface of concentration colored by windspeed. Blue shades indicate slower wind speeds and red shades indicate faster speeds.

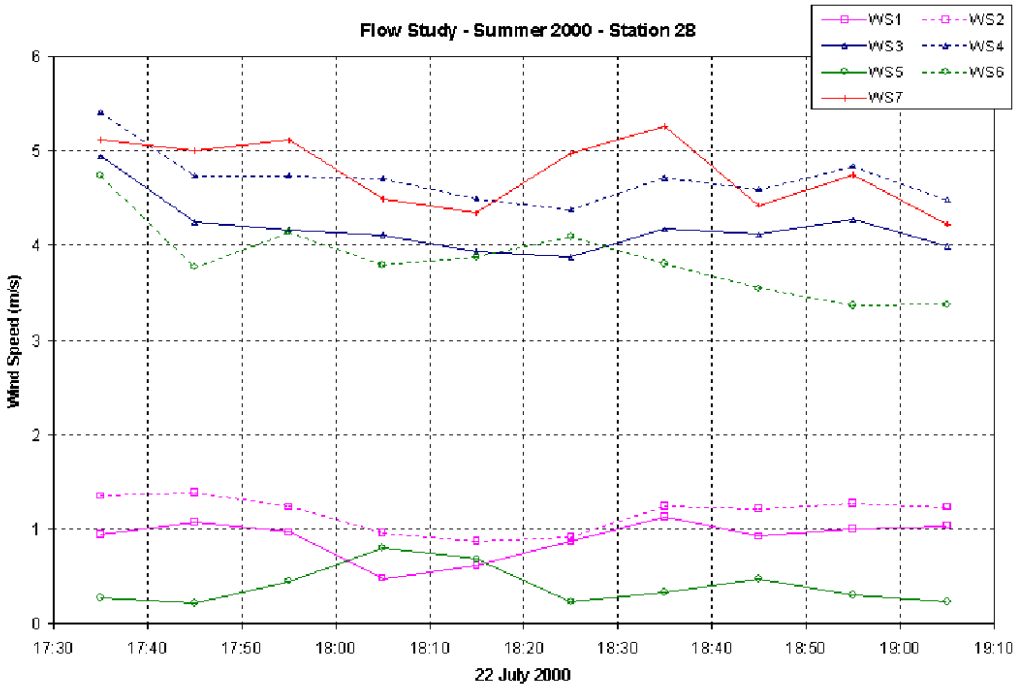

Figure 6. Ten minute averages of wind speed for all HS stations July 22, 2000.

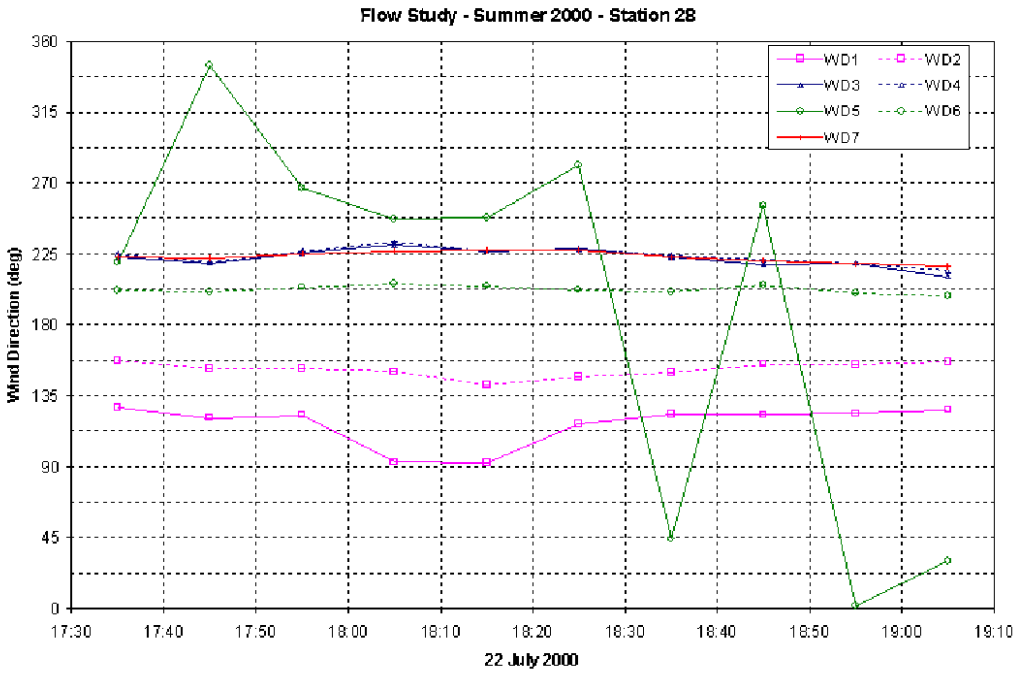

Figure 7. Ten minute averages of wind direction for all HS stations July 22, 2000.

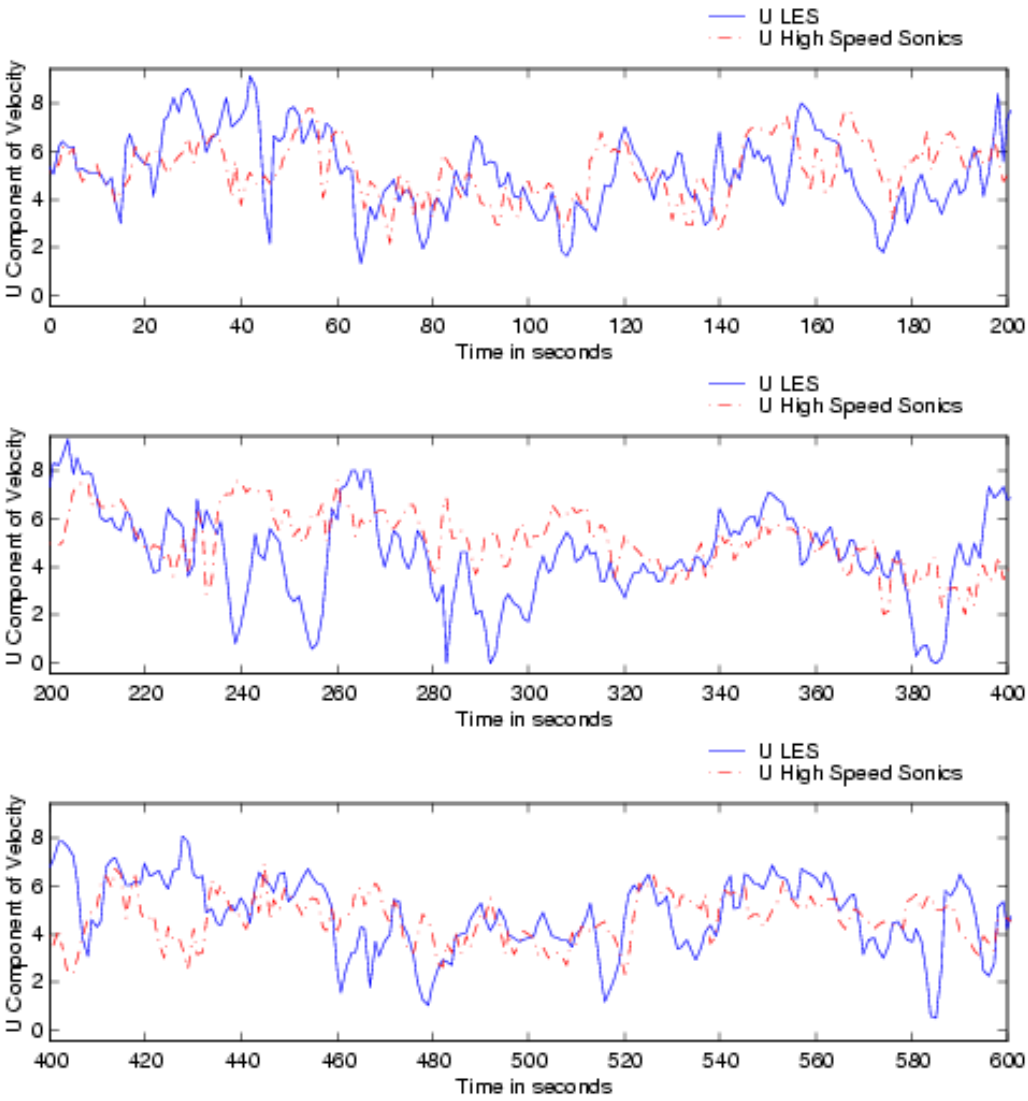

Figure 8. Simulated vs measured u component of velocity - high speed station 7.

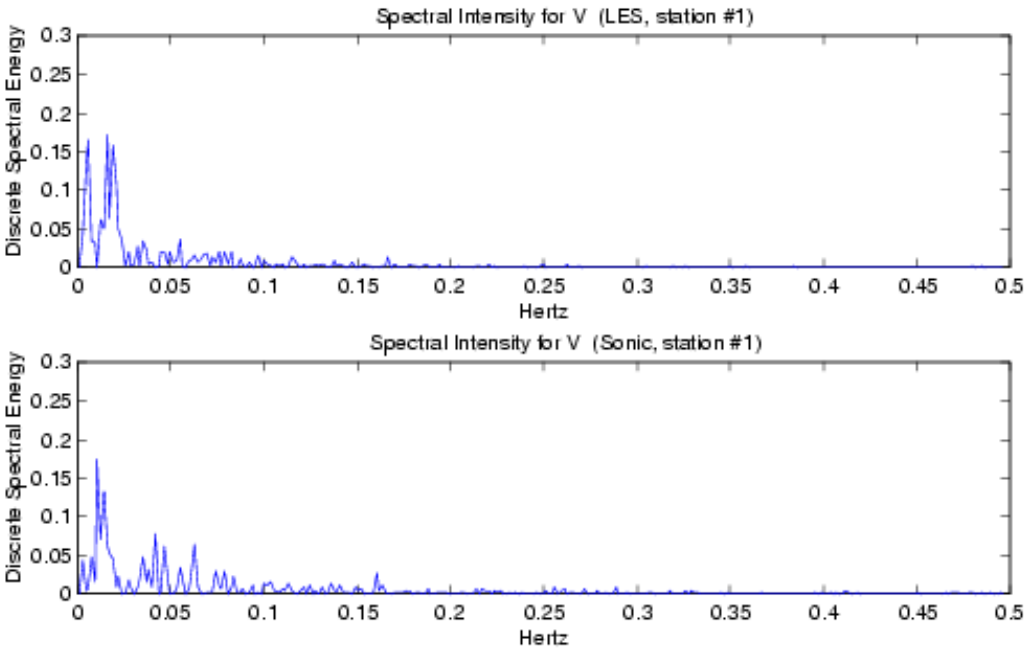

Figure 9. Spectra intensity v: simulated vs measured - high speed station 1.

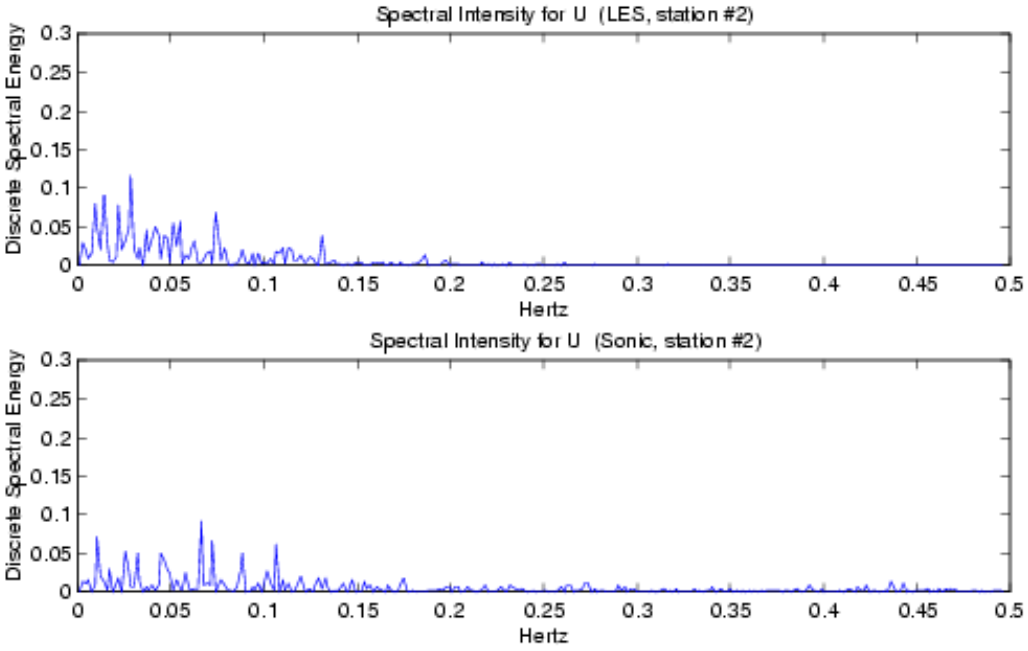

Figure 10. Spectra intensity u: simulated vs measured - high speed station 2.

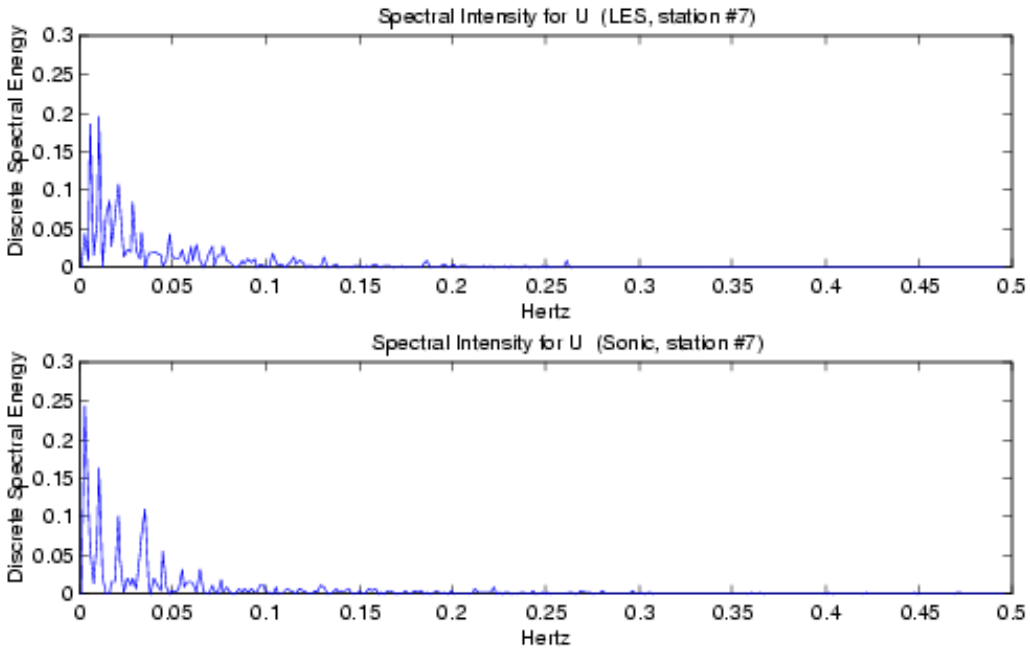

Figure 11. Spectra intensity u: simulated vs measured - high speed station 7.

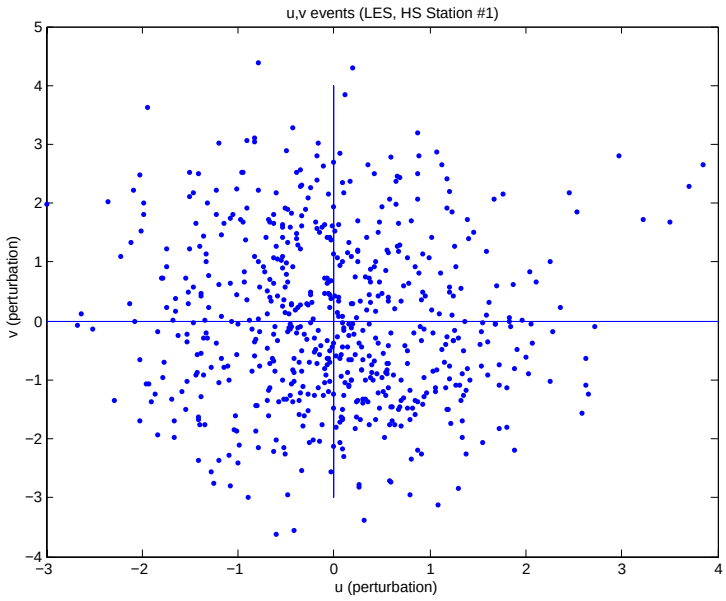

Figure 12. uv events: simulated - high speed station 1.

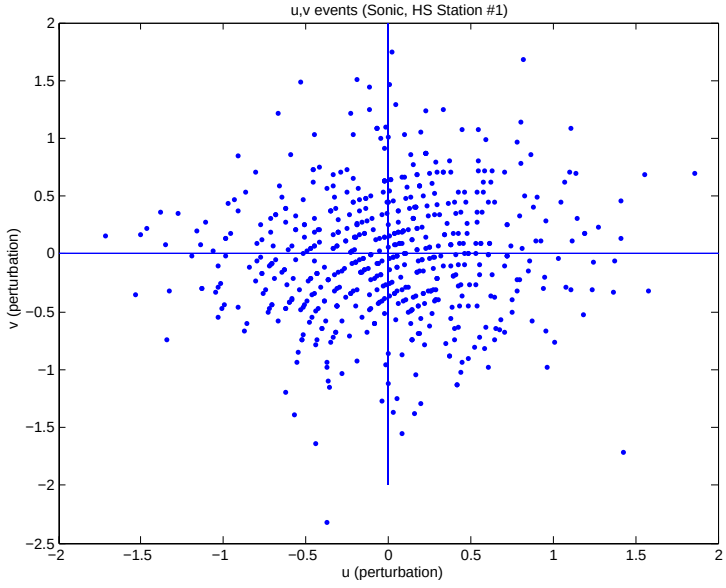

Figure 13. uv events: measured - high speed station 1.

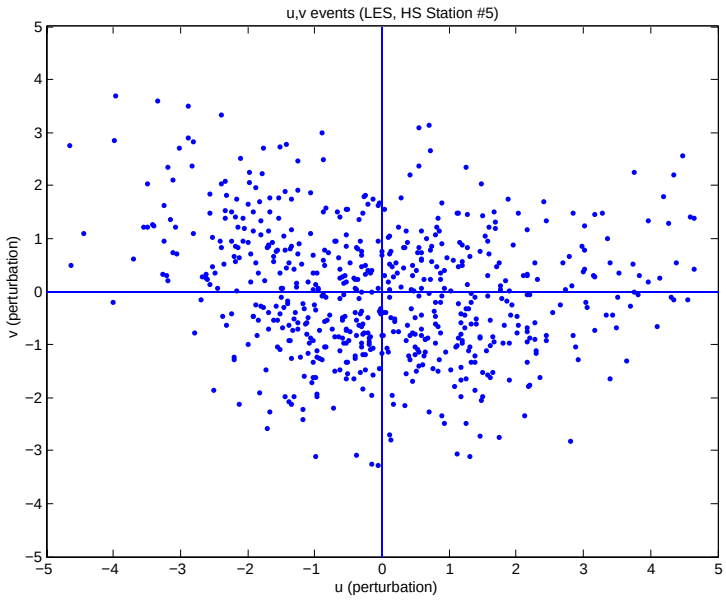

Figure 14. uv events: simulated - high speed station 5.

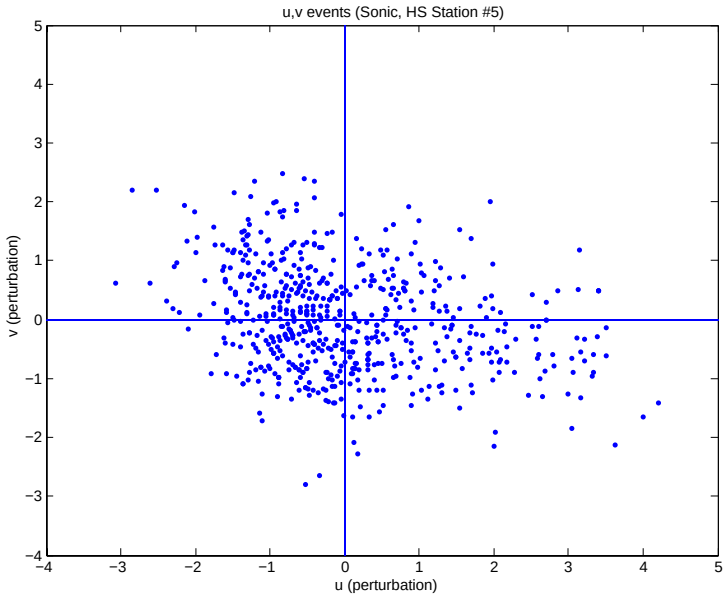

Figure 15. uv events: measured - high speed station 5.

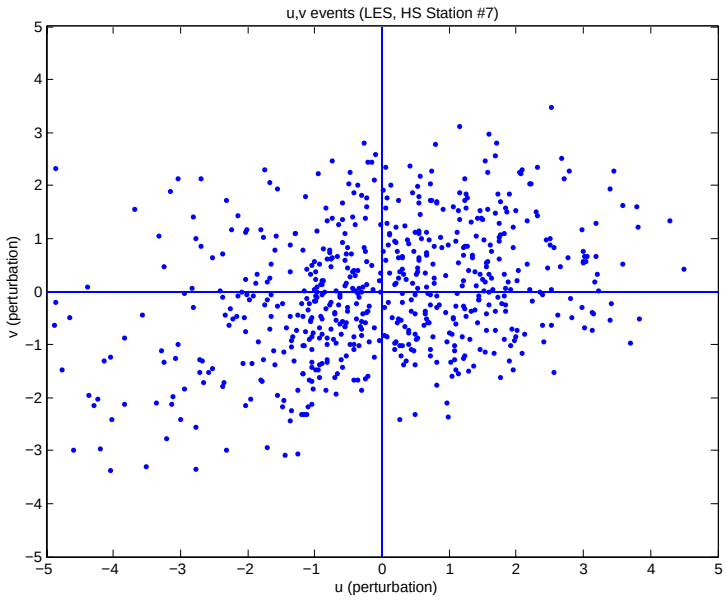

Figure 16. uv events: simulated - high speed station 7.

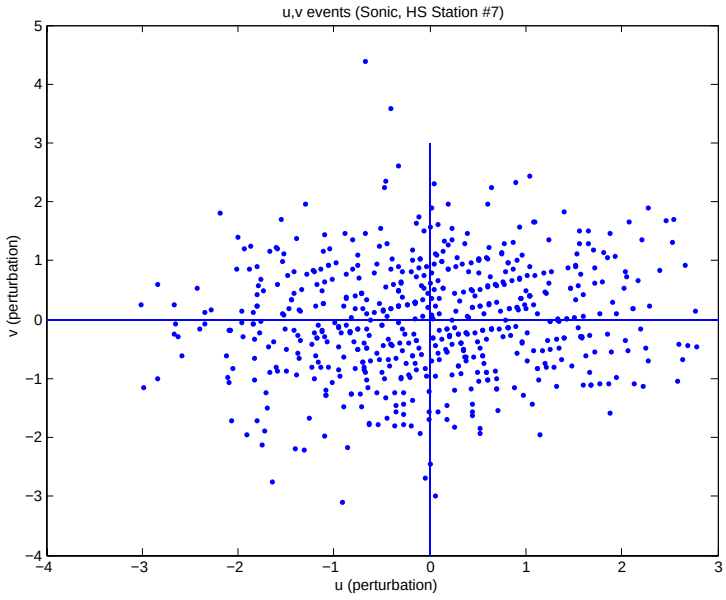

Figure 17. uv events: measured - high speed station 7.

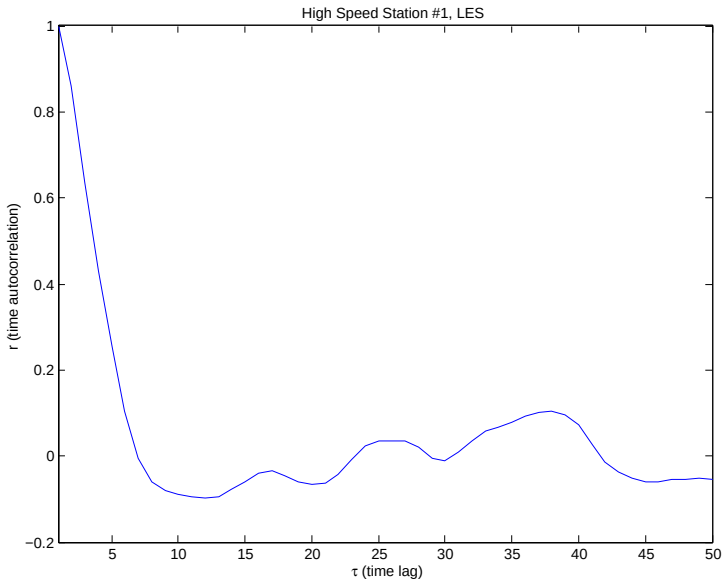

Figure 18. Autocorrelations of u in time: simulated - high speed station 1.

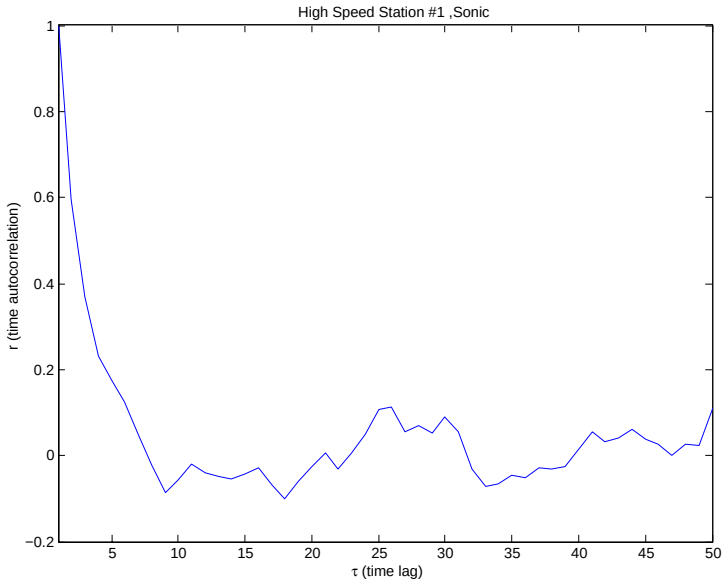

Figure 19. Autocorrelations of u in time: measured - high speed station 1.

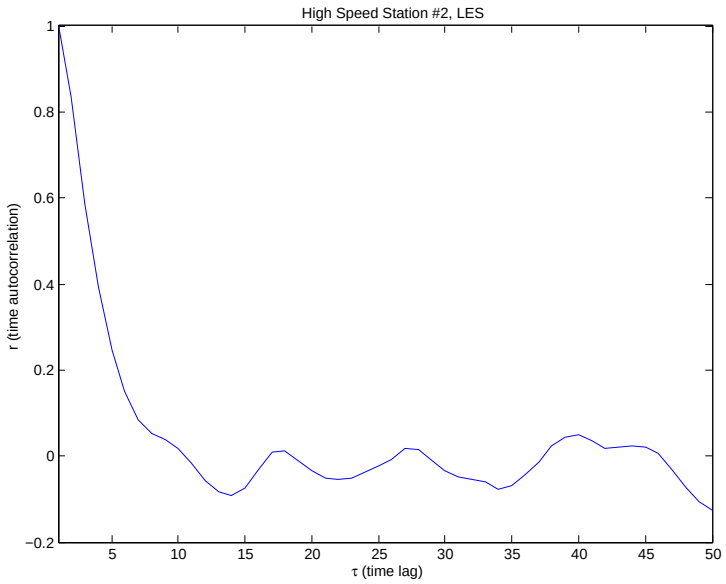

Figure 20. Autocorrelations of u in time: simulated - high speed station 2.

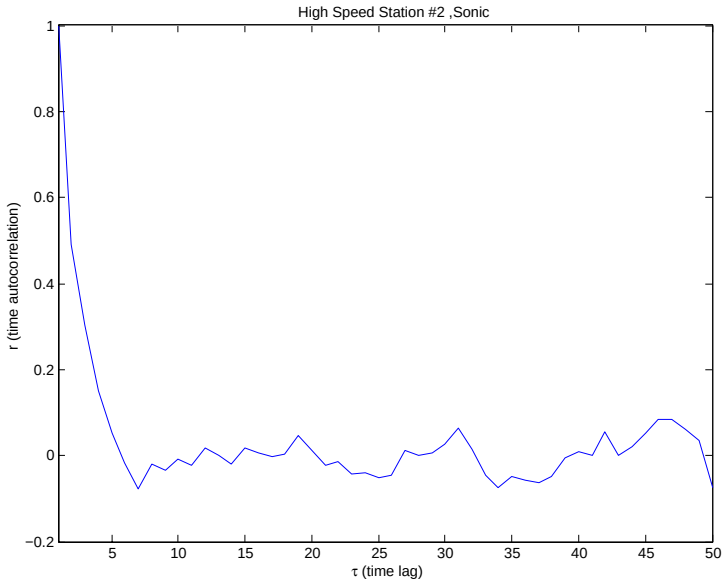

Figure 21. Autocorrelations of u in time: measured - high speed station 2.

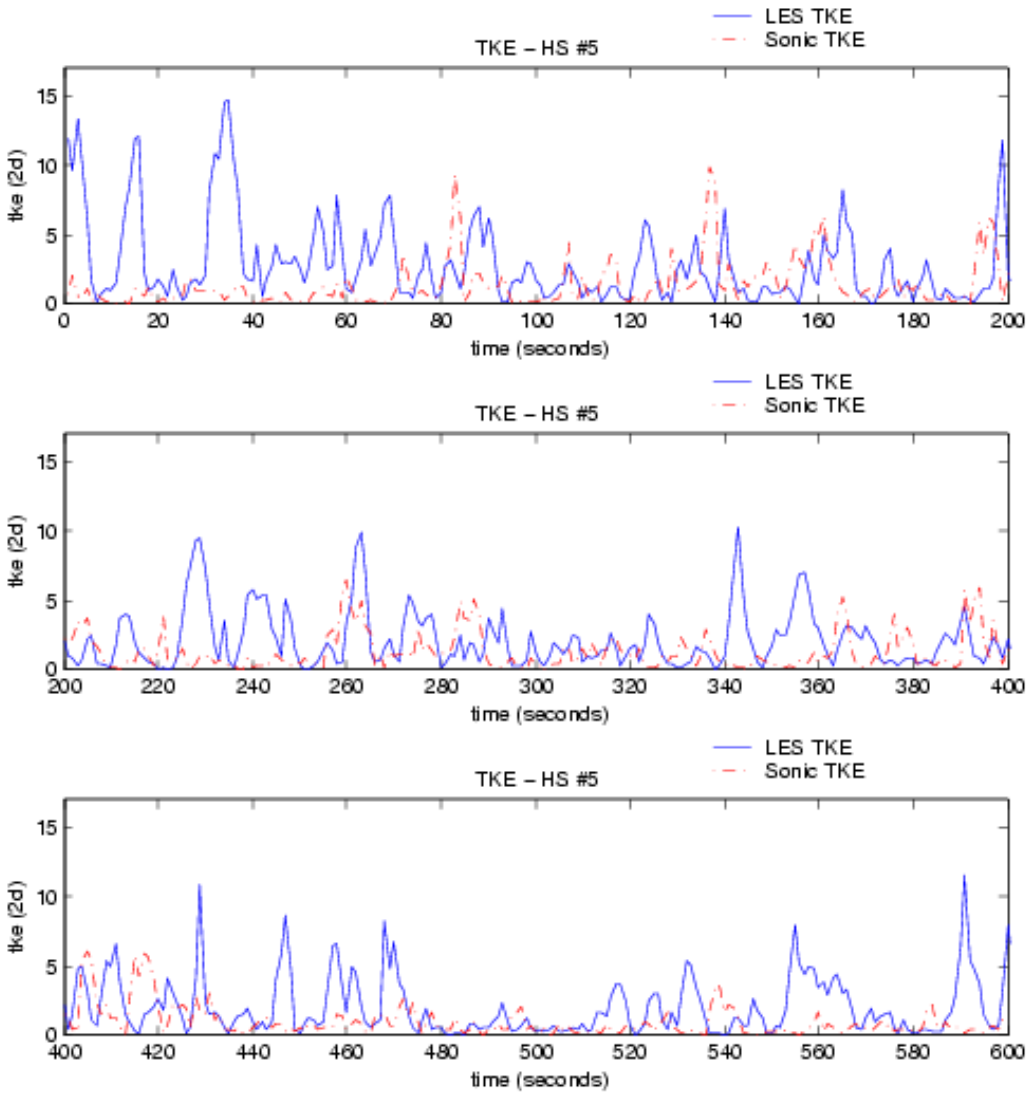

Figure 22. $\frac{1}{2}(\overline{u'u'} + \overline{v'v'})$: simulated vs measured - high speed station 5.

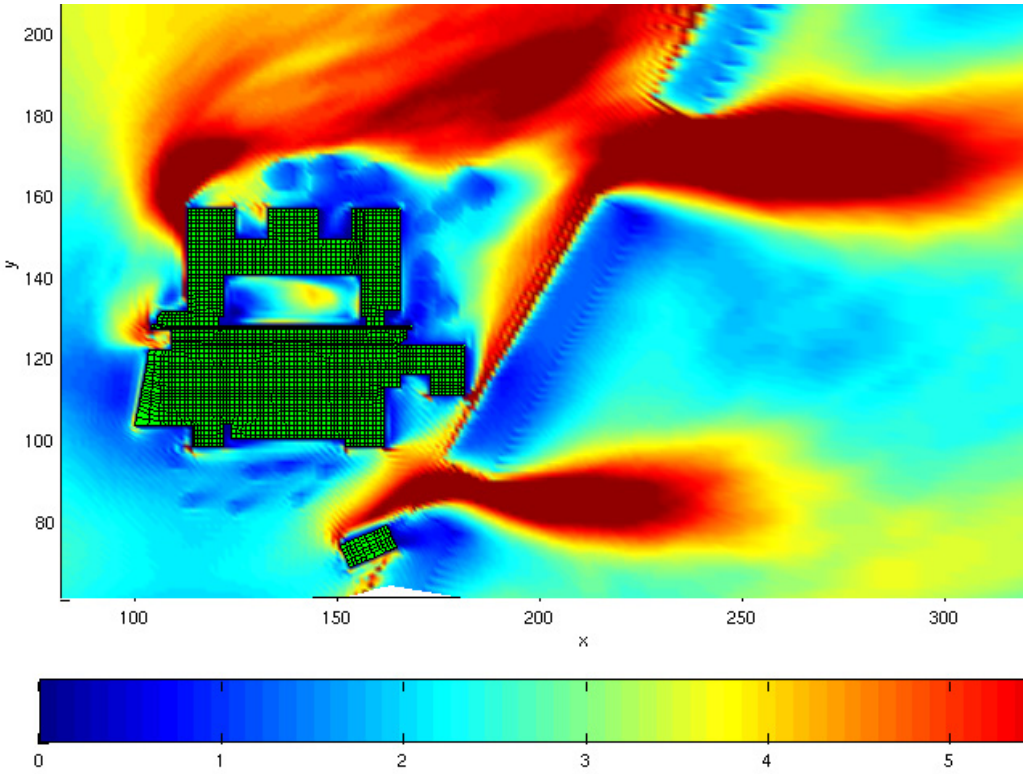

Figure 23. $\frac{1}{2}(\overline{u'u'} + \overline{v'v'})$: simulated. The vertical level of the horizontal plane depicted is 2.5 meters above the ground.

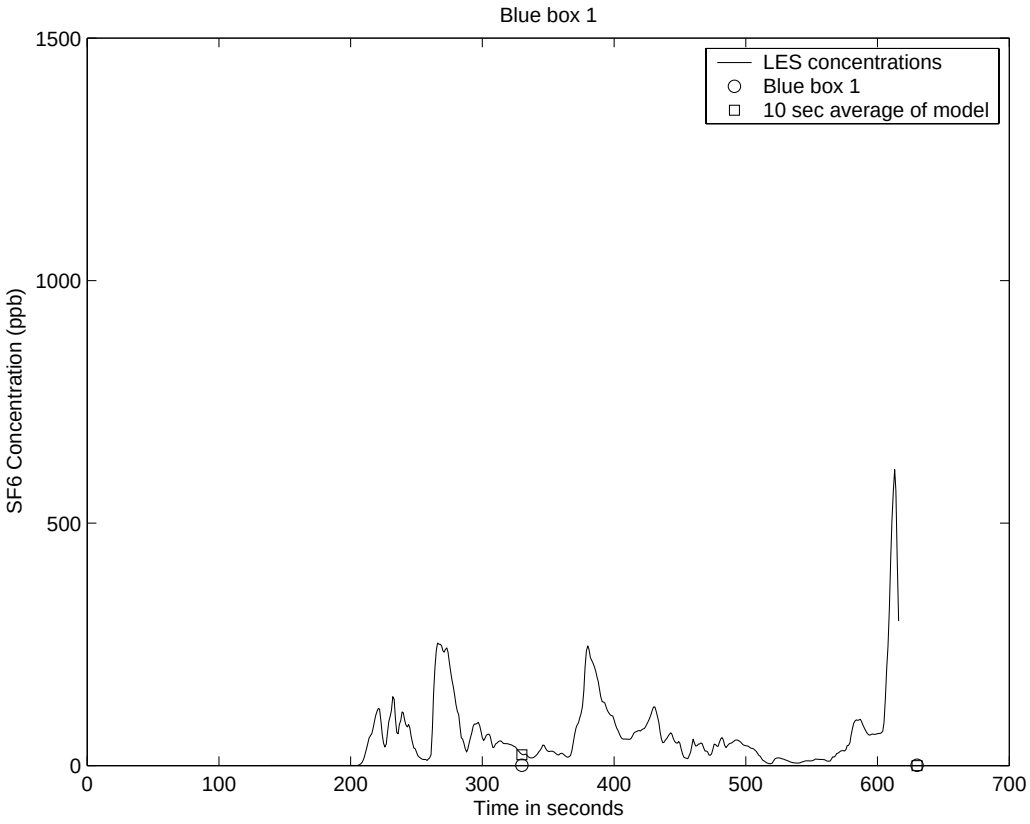

Figure 24. Concentrations of SF6 (ppb): simulated vs measured - BlueBox station 1.

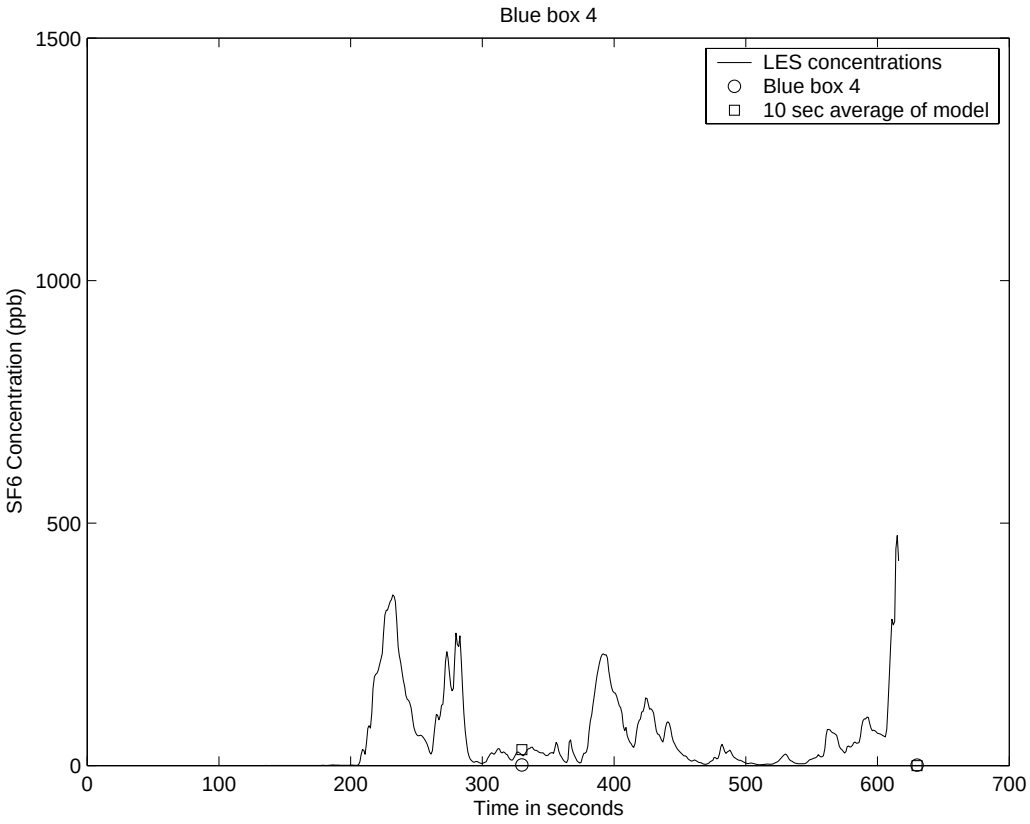

Figure 25. Concentrations of SF6 (ppb): simulated vs measured - BlueBox station 4.

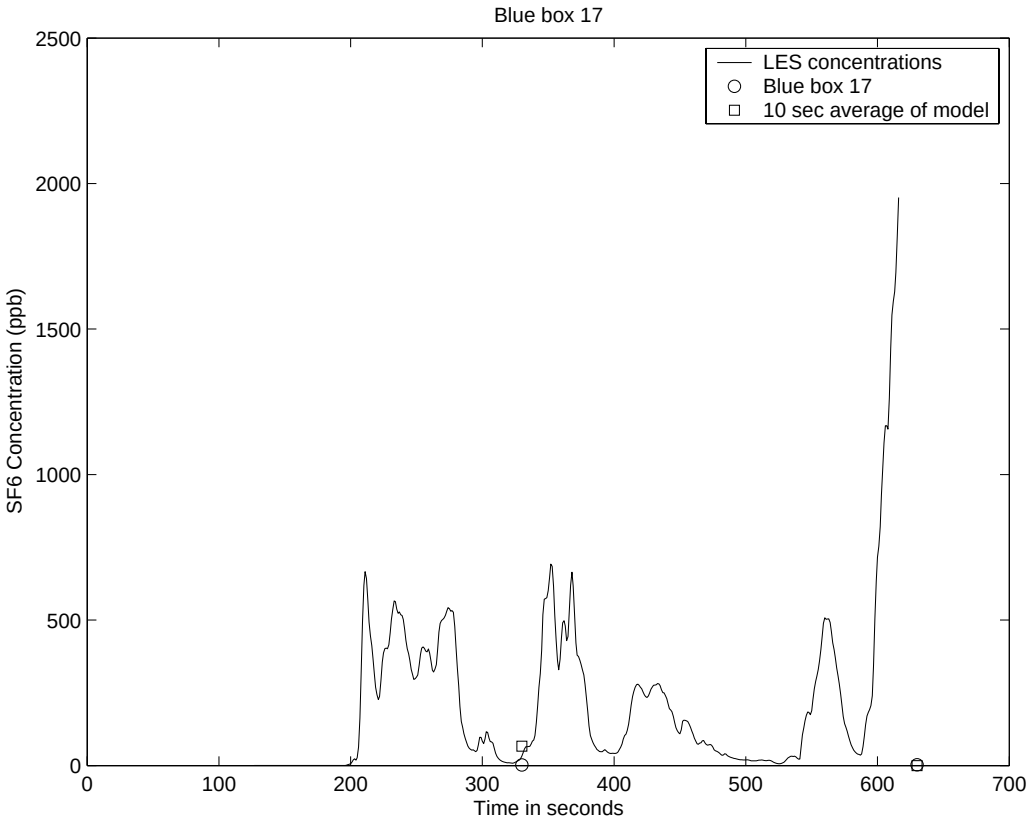

Figure 26. Concentrations of SF6 (ppb): simulated vs measured - BlueBox station 17.

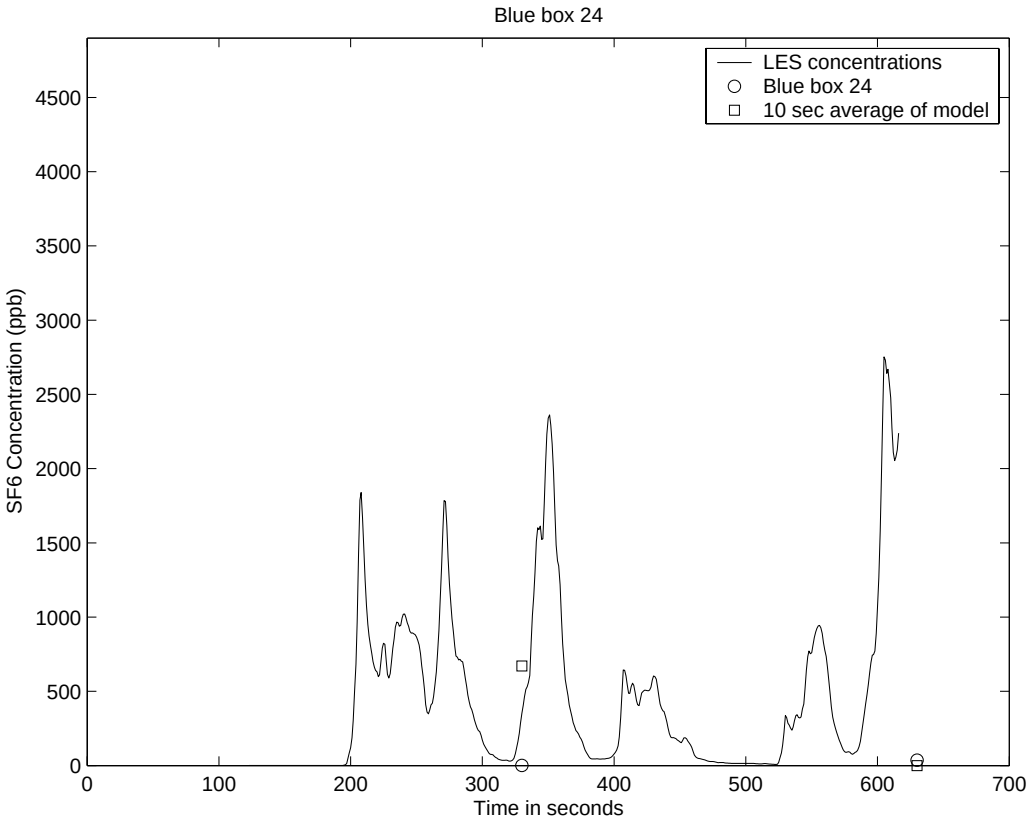

Figure 27. Concentrations of SF6 (ppb): simulated vs measured - BlueBox station 24.

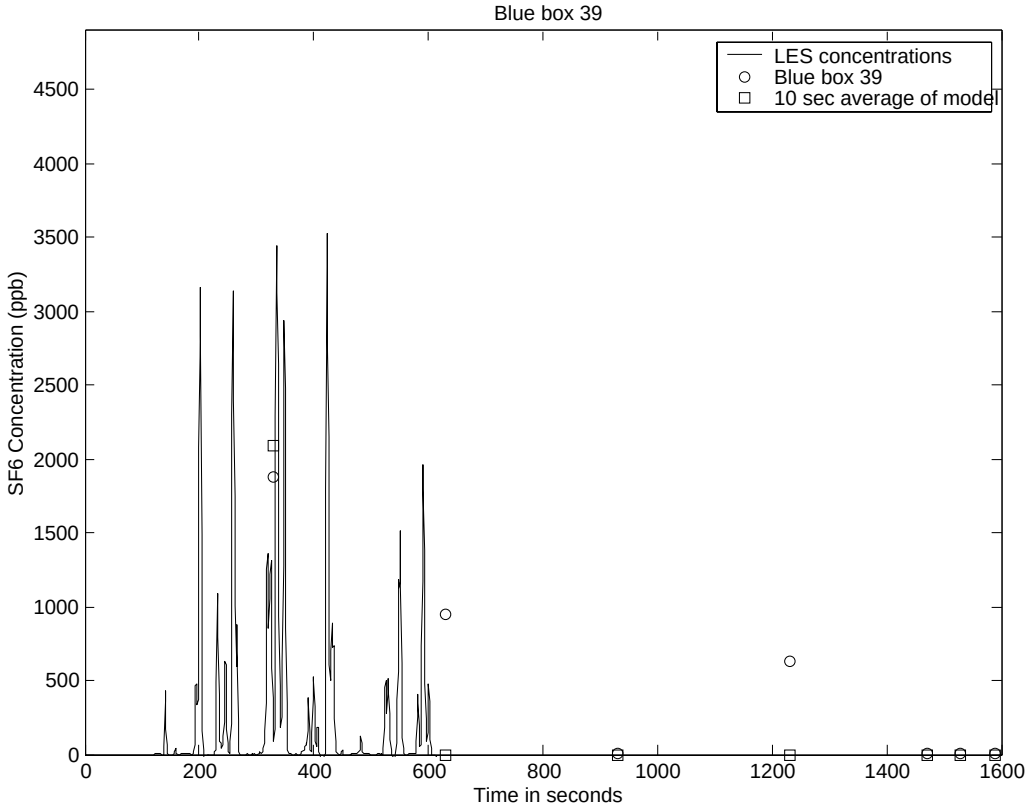

Figure 28. Concentrations of SF6 (ppb): simulated vs measured - BlueBox station 39. Note that even though the simulation did not extend this long, a longer time is shown on the x-axis to show how this blue box measured a significant amount of SF6 at 1200 seconds.

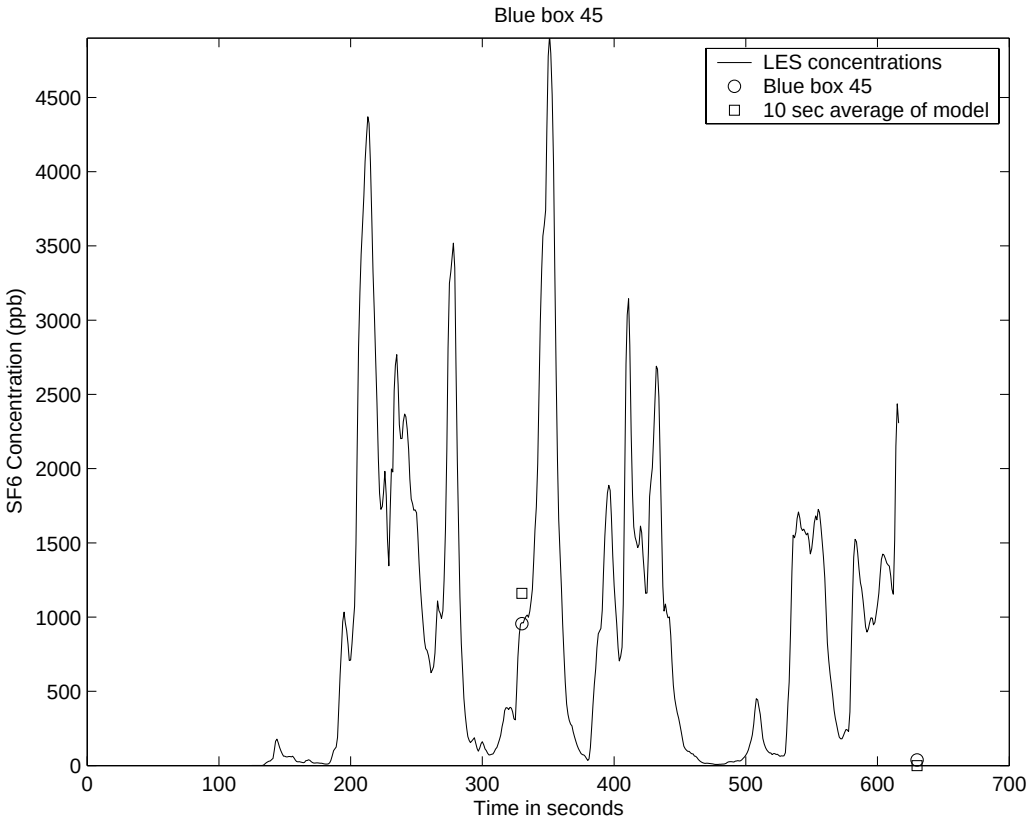

Figure 29. Concentrations of SF6 (ppb): simulated vs measured - BlueBox station 45.

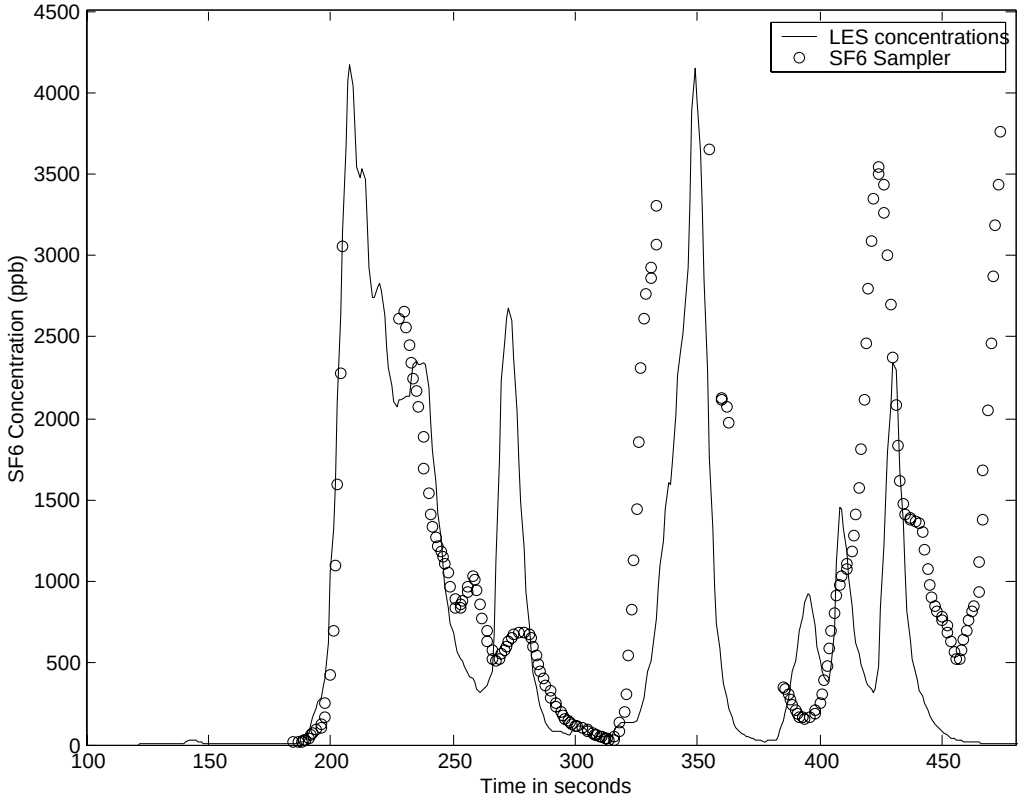

Figure 30. Real-time SF6 sampler vs LES - concentrations of SF6 (ppb). (Time range where both sets of data are available is shown.)

Table 1. Sampling for outdoor blue boxes - 7/22/00

Inside boxes		**Outside boxes**	
Time	Event	Time	Event
6:30	Release begun	6:30	Release begun
6:33	1st bag filled	6:33	1st bag filled
6:38	2nd bag filled	6:38	2nd bag filled
6:43	3rd bag filled	6:43	3rd bag filled
6:45	Release stopped	6:45	Release stopped
6:48	4th bag filled	6:48	4th bag filled
6:52	5th bag filled	6:55	5th bag filled
6:53	6th bag filled	7:00	6th bag filled
6:54	7th bag filled	7:15	7th bag filled

Table 2. Summary of Releases of SF_6 in Summer 2000

Test	Date	Start (PDT)	Duration (m:s)	Test	Date	Start (PDT)	Duration (m:s)
1	7/8	12:04	7:00	29	7/16	16:41	3:00
10	7/8	20:13	3:00	30	7/16	16:46	3:00
12	7/9	18:24	3:00	31	7/16	16:51	3:00
13	7/9	18:39	3:00	32	7/16	17:29	3:00
14	7/9	18:50	4:00	33	7/16	18:46	3:00
15	7/9	19:02	3:00	34	7/16	18:51	3:00
16	7/9	19:14	3:00	35	7/16	19:00	3:00
17	7/9	19:28	3:00	36	7/16	19:21	3:00
18	7/9	19:39	3:00	37	7/16	19:26	3:00
19	7/15	19:21	3:00	38	7/16	19:30	3:00
20	7/15	19:46	3:00	39	7/16	19:34	3:00
21	7/15	19:53	3:00	40	7/16	19:45	3:00
22	7/15	20:11	3:00	41	7/16	19:49	3:00
23	7/15	20:19	3:00	42	7/16	20:00	3:00
24	7/15	20:36	1:39	43	7/16	20:04	3:00
25	7/15	20:41	36:30	44	7/16	20:10	8:15
26	7/16	15:57	3:00	45	7/16	20:18	2:45
27	7/16	16:13	3:00	46	7/16	20:22	3:00
28	7/16	16:36	3:00	47	7/16	20:28	3:00
48	7/16	20:33	3:00	49	7/22	18:30	14:09

Table 3. Heights of Instruments - 8/22/00

Instrument	**vertical height**	**Instrument**	**vertical height**
Blue Box 1	1 meter	Blue Box 45	1 meter
Blue Box 4	1 meter	High Speed Sonic 1	2.5 meters
Blue Box 12	1 meter	High Speed Sonic 2	2.5 meters
Blue Box 17	1 meter	High Speed Sonic 3	4.4 meters
Blue Box 18	1 meter	High Speed Sonic 4	8.8 meters
Blue Box 23	1 meter	High Speed Sonic 5	2.5 meters
Blue Box 24	1 meter	High Speed Sonic 6	2.5 meters
Blue Box 39	10 meters	High Speed Sonic 7	14.02 meters
Miran Sampler	1 meter	SF_6 Source	Ground Level

Table 4. Statistical Comparison: LES vs Sonics - 8/22/00

	$\overline{u}$		$\overline{v}$		$\overline{u'u'}$		$\overline{v'v'}$		$\overline{u'v'}$		$r_{LES-Sonic}(u)$
Station #	LES	Sonic	LES	Sonic	LES	Sonic	LES	Sonic	LES	Sonic	corr. coef.
HS 1	-0.7	-0.5	0.6	1.0	1.1	0.3	2.0	.3	-0.1	0.0	-0.03
HS 2	-0.6	-0.0	2.0	1.2	1.1	0.5	2.2	0.6	-0.2	0.1	0.04
HS 5	-0.2	-0.3	-0.4	-0.1	3.2	1.6	1.5	.8	-0.4	-0.3	0.02
HS 6	1.4	3.0	4.2	2.5	1.7	0.6	3.5	0.8	1.4	-0.2	0.00
HS 7	4.9	5.0	2.0	1.5	2.9	1.3	1.5	0.9	0.7	0.1	0.22